Neuron
Article

ADF/Cofilin-Mediated Actin Retrograde Flow Directs Neurite Formation in the Developing Brain

Kevin C. Flynn,[1,2] Farida Hellal,[2] Dorothee Neukirchen,[1] Sonja Jacob,[3] Sabina Tahirovic,[1,4] Sebastian Dupraz,[2] Sina Stern,[2] Boyan K. Garvalov,[1,5] Christine Gurniak,[6] Alisa E. Shaw,[7] Liane Meyn,[1,2] Roland Wedlich-Söldner,[8] James R. Bamburg,[7] J. Victor Small,[3] Walter Witke,[6] and Frank Bradke[1,2,*]
[1]Max Planck Institute of Neurobiology, Axonal Growth and Regeneration Group, Am Klopferspitz 18, 82152 Martinsried, Germany
[2]German Center for Neurodegenerative Diseases (DZNE), Axonal Growth and Regeneration, Ludwig-Erhard-Allee 2, 53175 Bonn, Germany
[3]Institute of Molecular Biotechnology, Austrian Academy of Sciences, Dr. Bohrgasse 3, A-1030 Vienna, Austria
[4]German Center for Neurodegenerative Diseases (DZNE), Schillerstrasse 44, 80336 Munich, Germany
[5]Institute of Neuropathology, Justus Liebig University, Aulweg 123, 35392 Giessen, Germany
[6]Institute of Genetics, University of Bonn, Karlrobert-Kreiten Strasse 13, 53115 Bonn, Germany
[7]Department of Biochemistry and Molecular Biology, Colorado State University, 1870 Campus Delivery, Fort Collins, CO 80523, USA
[8]Cellular Dynamics and Cell Patterning Group, Max Planck Institute of Biochemistry, Am Klopferspitz 18, 82152 Martinsried, Germany
*Correspondence: frank.bradke@dzne.de
http://dx.doi.org/10.1016/j.neuron.2012.09.038

SUMMARY

Neurites are the characteristic structural element of neurons that will initiate brain connectivity and elaborate information. Early in development, neurons are spherical cells but this symmetry is broken through the initial formation of neurites. This fundamental step is thought to rely on actin and microtubule dynamics. However, it is unclear which aspects of the complex actin behavior control neuritogenesis and which molecular mechanisms are involved. Here, we demonstrate that augmented actin retrograde flow and protrusion dynamics facilitate neurite formation. Our data indicate that a single family of actin regulatory proteins, ADF/Cofilin, provides the required control of actin retrograde flow and dynamics to form neurites. In particular, the F-actin severing activity of ADF/Cofilin organizes space for the protrusion and bundling of microtubules, the backbone of neurites. Our data reveal how ADF/Cofilin organizes the cytoskeleton to drive actin retrograde flow and thus break the spherical shape of neurons.

INTRODUCTION

Neurons undergo dramatic morphological transformations during development. In the mammalian nervous system, they start out as simple symmetric spheres but develop into highly elaborate cells with distinct axonal and dendritic compartments (Rasband, 2010). For the latter stages of this process, progress has been made toward characterizing the mechanisms underlying axon and dendrite differentiation (Arimura and Kaibuchi, 2007; Barnes and Polleux, 2009; Stiess and Bradke, 2011). However, the first steps—when neurons initially transform from spheres to cells with neurites, the cylindrically shaped subcellular precursors of axons and dendrites (da Silva and Dotti, 2002)—remain enigmatic.

Neurites contain bundled microtubules and are tipped with an actin-rich growth cone (Conde and Cáceres, 2009). Past studies have identified essential features that turn nonneuronal cells into cells with neurite-like processes (Dehmelt et al., 2003; Edson et al., 1993). In hepatoma cells, overexpression of the neuron-specific microtubule-associated protein (MAP), MAP2c, generates microtubule bundles that, in conjunction with pharmacological depolymerization of cortical actin, enable neurite-like growth (Edson et al., 1993). This study raised the possibility that microtubule bundling and a dynamic cortical actin cytoskeleton, through which bundled microtubules protrude, could be the key intracellular processes underlying neurite formation. However, the events during neuritogenesis in neurons are still unclear. Moreover, it is unresolved which actin-dynamizing factors could regulate the cytoskeleton to enable neurite formation during brain development.

Studies of neuronal growth cones showed that the actin cytoskeleton undergoes an organized process of actin assembly/disassembly and actomyosin contractility to generate actin retrograde flow and growth cone translocation (Lowery and Van Vactor, 2009; Schaefer et al., 2008). The precise role of actin retrograde flow and the players involved in neuritogenesis are largely unknown. Several factors that directly or indirectly regulate actin dynamics have been proposed to facilitate neuritogenesis (da Silva and Dotti, 2002). For example, the actin filament anticapping factors, enabled/vasodilator-stimulated phosphoprotein (Ena/VASP), are important for neuritogenesis as mouse neurons lacking all three Ena/Vasp isoforms (Mena/VASP/EVL) remain spherical (Kwiatkowski et al., 2007). However, neurite formation can be restored in these neurons upon the activation of integrin signaling by plating them on laminin (Dent et al., 2007). This suggests that although Ena/VASP are important for mediating the signaling that elicits neurite formation, the intrinsic mechanism of neurite formation itself does not depend on Ena/VASP.

We have therefore searched for an actin-regulating factor that drives the intrinsic process of neurite formation. An important

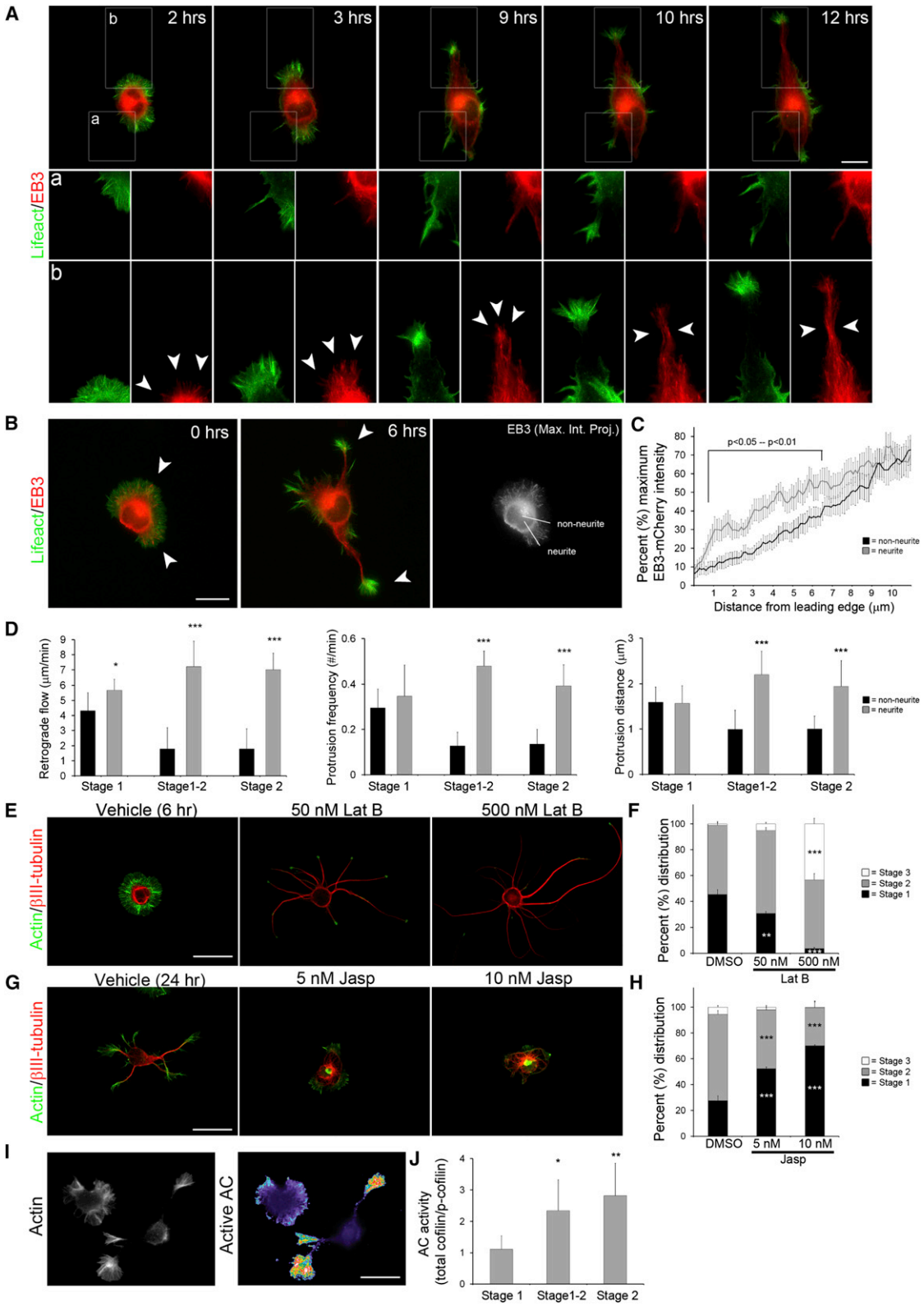

Figure 1. Actin Filament Organization and Dynamics Determine Neurite Formation

(A) Single frames of live-cell imaging of Lifeact-GFP and EB3-mCherry in a neuron undergoing neuritogenesis. The bottom panels show a magnified region from the top panels. Arrowheads indicate progressive bundling of microtubules over time. See also Movie S1. Scale bar represents 10 μm.

(legend continued on next page)

criterion for such a factor, deduced from the work of Edson et al. (1993), is that the candidate protein must enable F-actin disassembly and rearrangements that facilitate the protrusion of bundled microtubules out of the neuronal sphere to form a neurite. However, none of the proteins with strong actin filament-depleting activity studied so far affect neurite formation in physiological situations, including gelsolin (Lu et al., 1997). One prime candidate is the family of actin depolymerizing factor (ADF)/Cofilin (AC), which enhances actin dynamics in three ways: by depolymerization (accelerating monomer loss at the pointed end), by severing filaments into shorter protomers, and by directly or indirectly facilitating actin filament growth (Andrianantoandro and Pollard, 2006; Bernstein and Bamburg, 2010). AC proteins increase actin turnover in vitro (Carlier et al., 1997), enhance actin retrograde flow in epithelial cells (Delorme et al., 2007), and positively regulate growth cone dynamics in dorsal root ganglion neurons (Endo et al., 2003). Of the three mammalian AC family isoforms found in mammals, ADF and Cofilin-1 are both expressed in the mammalian brain with Cofilin-1 (hereafter simply "Cofilin") as the dominant isoform (Bellenchi et al., 2007). However, the genetic deletion of *Cofilin* in the nervous system reduces neuronal cell proliferation and migration but not neurite formation (Bellenchi et al., 2007). Moreover, the genetic ablation of *ADF* affects neither the development of the nervous system, nor the formation of neurites in particular (Bellenchi et al., 2007). Thus, so far, no actin filament modulator has been identified that regulates physiological neuritogenesis.

Here, we observed that increased actin dynamics are correlated with and necessary for the emergence of neurites out of the neuronal sphere. Although required for neuritogenesis, microtubules mainly follow the lead of the progressively dynamic actin cytoskeleton. Genetic ablation of a single family of actin-regulating proteins, ADF and Cofilin (hereafter "AC KO"), resulted in a failure of neuritogenesis due to profound cytoskeletal aberrations, including a blockade of F-actin retrograde flow and irregular microtubule growth. In the absence of AC proteins, pharmacological depolymerization of actin filaments enabled bundled microtubules to penetrate through the cell rim leading to neurite formation. The actin-severing activity was primarily linked to actin retrograde flow and neurite formation. We conclude that AC regulates neuritogenesis by driving actin turnover and organization, which is necessary for microtubule penetration and coalescence.

RESULTS

Neuritogenesis Requires Actin Turnover

We sought to characterize actin and microtubule dynamics during neurite formation. To date, such studies were hampered by the fact that fluorescently labeled actin could only be repetitively imaged in primary mammalian neurons for short time periods or with low temporal resolution (Dent et al., 2007; Flynn et al., 2009). We therefore used neurons from Lifeact-GFP mice, which exhibited stable green fluorescent protein (GFP) fluorescence to visualize actin dynamics with minimal photobleaching and phototoxicity (Riedl et al., 2010). To track polymerizing microtubules, we transfected Lifeact-GFP neurons with mCherry-tagged end-binding protein 3 (EB3-mCherry) (Akhmanova and Steinmetz, 2008). Within hours after plating, neurons assumed a characteristic "fried-egg" morphology (stage 1) (Dotti et al., 1988), with a circumferential actin-rich lamellipodium exhibiting moderate motility (Figure 1A, see Movie S1 available online). During neuritogenesis, filopodia became engorged with growing microtubules, expanded a growth cone, and progressed into a nascent neurite (Figure 1A). In addition, broad actin-based growth cone-like structures became more active and began advancing away from the soma, extending the membrane in their wake, which consolidated into a nascent neurite (Figure 1A). Initially, splayed microtubules closely trailed advancing actin structures and later coalesced into bundles as the neurite took shape (Figures 1A and S1A, Movie S1). Before neurite formation, microtubules advanced further into the periphery in neurite-forming zones compared to nonneurite-forming regions (Figures 1B and 1C). As neurite formation commenced (stage 1-2), the F-actin structures in nonneurite regions largely abated into stable, cortical actin in stark contrast to extending neurites, which displayed lamellipodia and filopodia with augmented dynamics (Figure S1B). Actin retrograde flow was higher in neurite-forming zones (7.2 ± 1.7 μm/min) compared to regions that did not

(B) Live-cell imaging of Lifeact-GFP and EB3-mCherry in a neuron undergoing neuritogenesis. Arrowheads indicate future sites of neurite formation. The right panel shows a maximum intensity projection of EB3-mCherry over 3 min. The lines indicate sites where line scans were taken for a neurite-forming region and a nonneurite-forming region. Scale bar represents 10 μm.
(C) The graph displays the average normalized intensity values of line scans of EB3-mCherry maximum intensity projections in neurite-forming zones compared to nonneurite-forming regions in stage 1 cells; n = 10.
(D) The bar graphs display quantifications of the average retrograde flow, protrusion frequency, and protrusion distance in neurite-forming zones compared to nonneurite-forming regions in stage 1, stage 1-2, and stage 2 cells; n = 8.
(E) The treatment of stage 1 neurons with latrunculin B accelerates neurite formation. Fluorescent staining for βIII tubulin and F-actin with fluorescent phalloidin is shown. Scale bar represents 20 μm.
(F) Quantification of the developmental stage of neurons with the indicated treatments. Stage 1, no neuritis; stage 2, minor neuritis; stage 3, axon and minor neurites (Dotti et al., 1988); n ≥ 250 cells from three separate experiments.
(G) The treatment of stage 1 neurons with jasplakinolide attenuates neurite formation. Fluorescent staining for βIII tubulin and F-actin with fluorescent phalloidin is shown. Scale bar represents 20 μm.
(H) Quantification of the developmental stage of neurons with the indicated treatments; n ≥ 200 cells from three separate experiments.
(I) ADF/Cofilin activity in stage 2 neurons compared to stage 1 neurons shown by ratio of total Cofilin and phosphorylated Cofilin. Warmer colors represent higher ratios. F-actin is stained with fluorescent phalloidin. Scale bar represents 20 μm.
(J) Quantification of average Cofilin activity; n ≥ 75 cells from three separate experiments.
**p < 0.01, **p < 0.01, ***p < 0.001. Error bars represent SD.

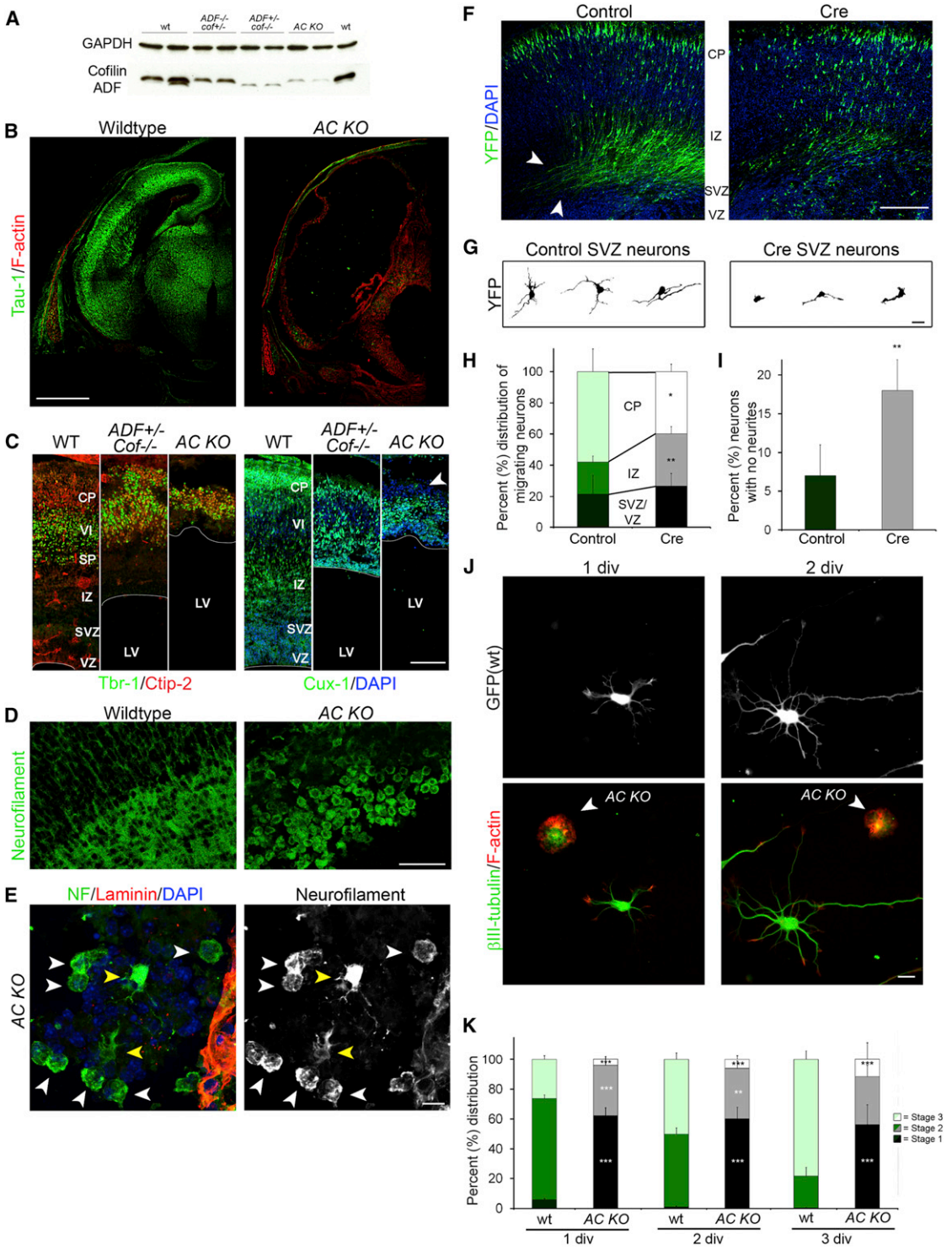

Figure 2. ADF/Cofilin Is Necessary for Neuritogenesis

(A) Western blot of E17 cortex from wild-type (WT), conditional (*nestin-cre*) *cofilin* monoallele (ADF$^{-/-}$,Cof$^{+/-}$), *ADF* monoallele (*ADF*$^{+/-}$, *Cof*$^{-/-}$), and *ADF*/*Cofilin* double knockout (*AC KO*). ADF (bottom band) and Cofilin (top band) were both detected by a single antibody.

(B) Confocal micrographs of fluorescent stainings for Tau-1 (green) and F-actin (red) of E17 neocortical coronal sections from wild-type and *ADF*/*Cofilin* double knockout (*AC KO*) brains. Scale bar represents 1 mm.

(C) The left panels show confocal micrographs of Trb-1 (green, layer VI, preplate marker) and Ctip-2 (red, layer V, cortical plate marker) and the right panels show confocal micrographs of Cux-1 (green, VZ, SVZ, and cortical plate marker) and DAPI (blue, all cells) of E17 neocortical coronal sections from wild-type, *ADF*

(legend continued on next page)

form neurites (1.8 ± 1.4 μm/min, $p < 0.001$), actin-based membrane protrusions were more frequent (0.5 ± 0.1 protrusions/min versus 0.1 ± 0.1 protrusions/min, $p < 0.001$), and these protrusions extended a greater distance (2.2 ± 0.5 μm versus 1.0 ± 0.4 μm, $p < 0.001$) (Figure 1D). In addition, actin retrograde flow, protrusion frequency, and protrusion distance increased in neurite-forming regions in stage 1-2 and stage 2 neurons compared to stage 1 neurons (Figure S1C).

As microtubules protrude closer to the leading edge in neurite forming zones, where actin is also more dynamic, we wondered whether actin destabilization accelerates neurite formation. In fact, within 6 hr after plating, more than 95% of the neurons treated with 500 nM latrunculin B contained neurites. Hence, latrunculin treatment induced over a 12-fold decrease in the percent of neurons without neurites (3.7% ± 0.72% for 500 nM latrunculin B versus 45.5% ± 3.6% for DMSO, $p < 0.001$; Figures 1E and 1F). Moreover, local application of latrunculin B induced neurite protrusions at the site of actin destabilization (Figure S1D). Moderate microtubule stabilization by low doses of taxol, which induces supernumary axons in neurons already containing neurites (Witte et al., 2008), did not augment neurite formation (Figures S2A and S2B). To determine whether actin turnover is necessary for neuritogenesis, we treated stage 1 neurons with the F-actin stabilizing drug jasplakinolide. Nanomolar doses of jasplakinolide completely abolished retrograde flow after 1 hr (Figure S2C). At 5 nM jasplakinolide, neurons still displayed normal features of the actin cytoskeleton, including filopodia (Figure 1G). However, at 10 nM jasplakinolide, the organization of the cytoskeleton was disrupted with abnormal F-actin accumulations and looping microtubules. After 1 day in vitro (DIV), jasplakinolide-treated neurons largely failed to form neurites, resulting in a more than 2-fold increase in stage 1 cells (70.2% ± 1.4% for 10 nM jasplakinolide versus 27.7% ± 3.5% for DMSO, $p < 0.001$; Figure 1H). Thus, actin turnover is a critical regulator of neuritogenesis.

Neuritogenesis Requires ADF/Cofilin Proteins

We hypothesized that the activity of an endogenous factor underlies the observed increase in actin disassembly and turnover, facilitating the radial growth of microtubule bundles during neurite formation (Figure S2D). Proteins of the ADF/Cofilin (AC) family are prime candidates for such activity. Live-cell imaging experiments showed that neurons expressing Cofilin-RFP had increased retrograde flow rates compared to neurons expressing RFP (8.3 ± 1.4 μm/min versus 5.1 ± 0.6 μm/min for RFP control, $p < 0.001$, Figures S2E and S2F). Immunocytochemistry for active AC (ratio of total cofilin/phosphorylated cofilin) revealed that stage 2 growth cones had elevated AC activity compared to stage 1 cells (2.8 ± 1.0 versus 1.1 ± 0.4, $p < 0.01$; Figures 1I–1J).

To test the physiological role of AC proteins in neuritogenesis, we generated mice with brain-targeted deletion of both *ADF* and *Cofilin* (*AC KO*). We crossed *ADF KO* mice ($ADF^{-/-}$) with brain-specific *Cofilin KO* mice (*Nestin* $Cre^{+/-}$, *cofilin* $^{flox/flox}$) by standard genetic crossings (Bellenchi et al., 2007). The *AC KO* progeny were observed at expected Mendelian ratios at embryonic days 15–17 (E15–E17) but died within 12 hr after birth. Using an antibody that recognizes both ADF and Cofilin in mouse, we confirmed that ADF was undetectable while Cofilin had a slight residual expression in the *AC KO* at E17 due to intercalation of the meninges in the cortical tissue (Figures 2A and S3C). At this age, *AC KO* mice had multiple severe abnormalities in all areas of the brain compared to wild-type control brains. First, *AC KO* brains displayed drastic cortical hypoplasia and extreme ventricle expansion (Figures 2B, S3A, and S3B). Second, *AC KO* brains showed cortical ectopias, resembling the cobblestone-like cortex observed in type II lissencephaly, an archetypal neuronal migration disorder (Figure S3C) (Bielas et al., 2004). Consistent with a defect in neuronal migration, cortical lamination was drastically disrupted in the *AC KO* brains and neurons of the distinct layers were intermingled (Figures 2C and S3B). The brain morphology of the *ADF* monoallele (*NesCre*$^{+/-}$, *ADF*$^{+/-}$, *cofilin* $^{flox/flox}$) had a similar, though less profound, phenotype (Figures S3A and S3B). In contrast to the *ADF* monoallele, *cofilin* monoallele (*NesCre*$^{+/-}$, $ADF^{-/-}$, *cofilin* $^{flox/+}$) brains were morphologically indistinguishable from wild-type brains, as previously reported for *ADF KO* mice (data not shown) (Bellenchi et al., 2007).

Immunostaining with the axonal marker Tau-1 revealed that there were no obvious axonal tracts in the *AC KO* and the *ADF* monoallele brains, even in regions of the brain that remained intact (Figures 2B, S3A, and S3B). We confirmed the deleterious effects of AC ablation on cortical mass and axon tract

monoallele, and *ADF*/*Cofilin* double knockout (*AC KO*) brains. The markers are intermingled in the *AC KO* and to a lesser degree in the *ADF* monoallele. Cux1 is greatly reduced in the top layers of the cortex (arrowhead). Scale bar represents 200 μm.

(D) Confocal fluorescent micrographs of neurofilament staining of E17 wild-type and *AC KO* cortex. Scale bar represents 50 μm.

(E) Higher magnification of confocal fluorescent micrographs of E17 *AC KO* cortex. The *AC KO* neurons are mainly spherical and lack protrusions (white arrowheads). However, a few neurons have short neurites (yellow arrowheads). Scale bar represents 10 μm.

(F) Confocal fluorescent micrographs of E18.5 cortices transfected via in utero electroporation of $ADF^{-/-}$, $Cofilin^{flox/flox}$ brains at E14 with either YFP control vector or Cre + YFP vectors. The YFP (green) shows the individual transfected cells in control conditions (left) and in knockdown conditions (Cre expression, right). Long axonal tracts are formed by the control neurons (arrowheads), which are diminished in Cre-expressing neurons. Scale bar represents 200 μm.

(G) Camera lucida traces of individual cells from the SVZ of in utero electroporation experiments. Scale bar represents 20 μm.

(H) Quantification of the distribution of control (green tones) and Cre-transfected (gray tones) cells within the cortex. $n \geq 1480$ cells from five experiments.

(I) Quantification of cells with no neurites in the SVZ for control (YFP) and Cre (Cre + YFP) neurons. $n \geq 540$ cells from five experiments.

(J) Fluorescent micrographs of GFP, βIII tubulin, and F-actin of wild-type (GFP positive) and *ADF*/*Cofilin* knockout (*AC KO*, GFP negative, indicated with arrowheads) neurons at 1 day in vitro (1 DIV) and 2 DIV. Scale bar represents 10 μm.

(K) Stacked bar graph of neurite growth phenotypes in wild-type and *AC KO* neuronal cultures at different stages of development. $n \geq 500$ cells for each time point from four experiments.

*$p < 0.05$, **$p < 0.01$, ***$p < 0.001$. Error bars represent SD.

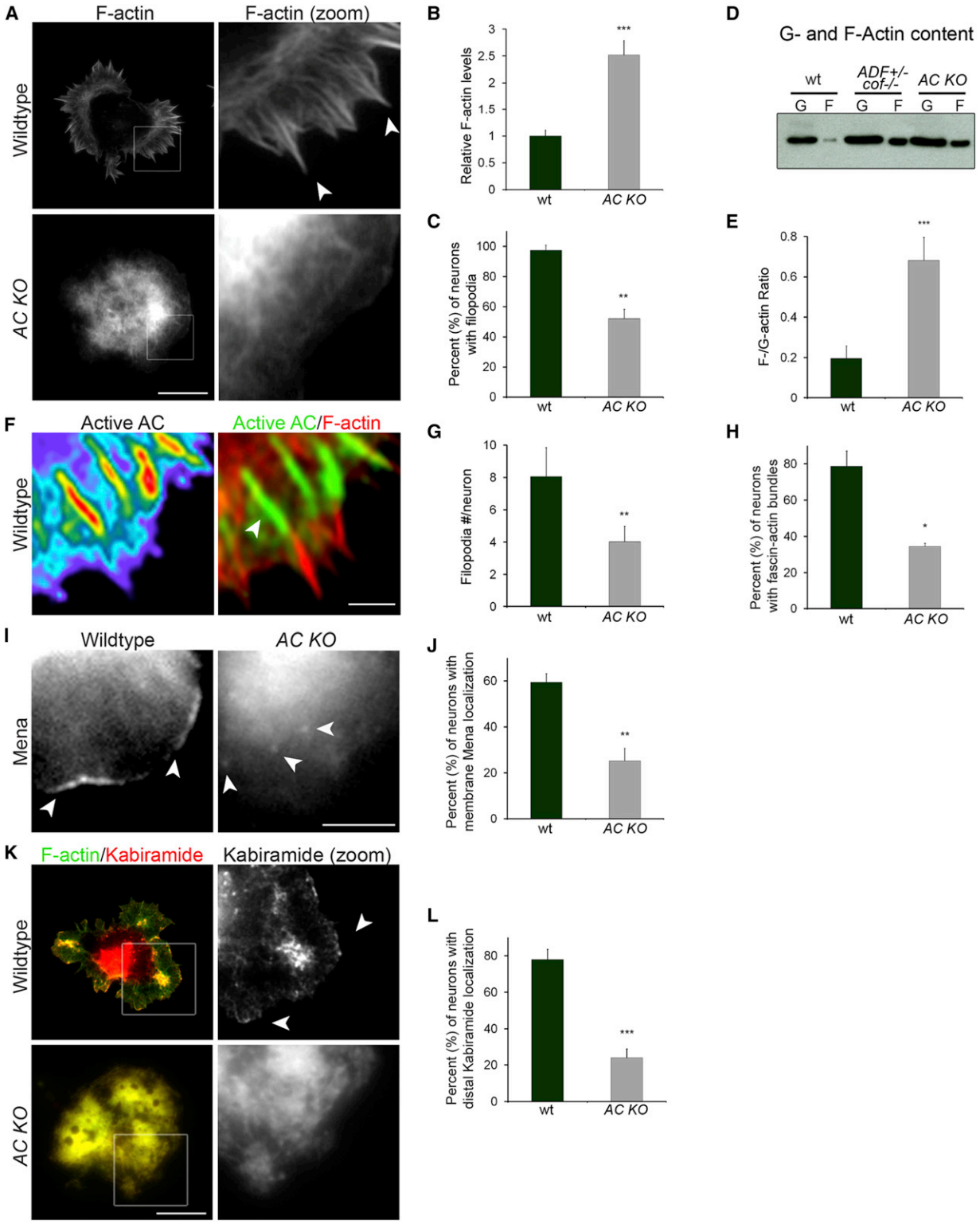

Figure 3. ADF/Cofilin Is Required for Actin Organization

(A) Fluorescent images of F-actin (phalloidin) in stage 1 wild-type and *AC KO* neurons. F-actin density and disorganization is increased in *AC KO* neurons. The right panels are magnified views of the indicated regions. Arrowheads indicate filopodia. Scale bar represents 10 μm.

(B) Quantification of relative F-actin levels indicates a 2.5-fold increase in *AC KO* neurons compared to wild-type neurons. The bar graph represents the averages of three experiments, n ≥ 120 cells for each group.

(legend continued on next page)

formation utilizing additional neuronal-specific promoters, Nexin (Goebbels et al., 2006) and Tau (Korets-Smith et al., 2004), to drive Cre expression (data not shown). Analysis of neurofilament-positive neurons at high resolution in vivo showed that the majority of *AC KO* neurons had remained spherical and lacked neurites, contrasting with the dense neurite network of wild-type neurons (Figures 2D and 2E).

To test whether the in vivo defects in neuritogenesis were caused by cell-intrinsic mechanisms, we electroporated *ADF*$^{-/-}$, *cofilin* $^{flox/flox}$ E14 embryos in utero with DNA vectors expressing Cre recombinase and yellow fluorescent protein (YFP) or GFP. In addition to irregular neuronal cell migration, Cre expression resulted in reduced axon tracts and altered neuronal morphogenesis 4 days after electroporation (E18) (Figures 2F–2I). In the subventricular zone (SVZ), where neurons exhibit a multipolar morphology with multiple long neurites (Barnes and Polleux, 2009) (Figure 2G), Cre-expressing neurons in the same regions either displayed short processes or completely lacked neurites (Figures 2F–2I).

Consistently, dissociated *AC KO* neurons that were plated together with GFP-labeled wild-type neurons (Garvalov et al., 2007) recapitulated the in vivo phenotype. While only 5.9% ± 0.7% of wild-type neurons had no neurites after 1 DIV, 62.2% ± 5.3% of *AC KO* neurons failed to elaborate neurites, a 10-fold increase ($p < 0.001$; Figures 2J and 2K). *AC KO* neurons did not experience a delayed development but rather a fundamental inhibition of neurite initiation as the number of *AC KO* neurons without neurites did not change significantly from 1–3 DIV (Figure 2K). Long-term live-cell imaging experiments showed that stage 1 wild-type neurons were dynamic and extended neurites within 8 hr after plating, while *AC KO* neurons were far less motile, only changing shape slowly and rarely forming neurites (Figure S4A). Downregulation of ADF and Cofilin in a neuronal cell line, N2A cells, also showed a stark decrease in neuritogenesis, affirming the data from the genetic knockout in primary neurons (data not shown). Together, these data show that AC proteins are essential for neurite formation during brain development.

AC Proteins Regulate F-Actin Content, Organization, and Filopodia Formation

We evaluated the structure of the cytoskeleton in *AC KO* neurons as the potential determinant regulating neuritogenesis (Dehmelt et al., 2003; Dent et al., 2007; Edson et al., 1993). *AC KO* brains and cultured *AC KO* neurons showed a striking increase in the intensity of phalloidin staining (Figures 2B, 3A, 3B, and S3A). This increase in F-actin was also detected in biochemical extracts of *AC KO* neurons (Figures 3D and 3E). Moreover, *AC KO* neurons presented an abnormal F-actin distribution typically with a strong F-actin staining in the center of the soma with irregular F-actin depositions in most regions, while some regions were devoid of F-actin. This contrasted the actin cytoskeletal structure of wild-type neurons, which showed organized, radial actin filaments in the periphery of the cell and were devoid of actin in the center (Figure 3A). *AC KO* neurons also formed less filopodia (Figures 3A, 3C, and 3G). Consistent with a role of AC proteins in filopodia dynamics, the highest level of AC activity was observed at the base of filopodia (Figure 3F). Furthermore, Fascin-GFP, a marker of filopodia and microspikes (Cohan et al., 2001), localized to radial actin bundles in filopodia of wild-type neurons but only showed a diffuse signal in *AC KO* neurons and rarely localized to filopodia-reminiscent structures (Figure 3H). Expression of Mena-mCherry, which was used as a marker for the barbed ends of actin filaments (Bear and Gertler, 2009), was localized at the cell edge in 59.3% ± 3.8% of the wild-type cells but only in 25.3% ± 5.4% of *AC KO* neurons ($p < 0.01$; Figures 3I–3J). Consistently, rhodamine-kabiramide, which binds directly to the barbed ends of actin filaments (Petchprayoon et al., 2005), localized in a distal-proximal gradient in wild-type cells but displayed dispersed staining throughout the soma of the KO neurons (Figures 3K and 3L). Taken together, these data indicate that the barbed end orientation toward the leading edge is disrupted in the *AC KO* neurons. Despite the abnormal barbed end distribution, Abi, an essential component of the WAVE complex, showed strong staining at the membrane of *AC KO* neurons (data not shown), indicating that WAVE-Arp2/3-mediated actin

(C) Quantification of the percentage of cells with filopodia in stage 1 wild-type and *AC KO* neurons. The results are from three experiments, $n \geq 150$ cells for each group.

(D) Western blot showing G- and F-actin levels in cultured wild-type, *ADF* monoallele (*ADF*$^{+/-}$, *Cof*$^{-/-}$), and *AC KO* neurons. F-actin increases in *ADF* monoallele (*ADF*$^{+/-}$, *Cof*$^{-/-}$) and *AC KO* neurons.

(E) Quantification of F-/G-actin ratios from three experiments.

(F) Ratio imaging of total Cofilin to phosphorylated Cofilin reveals localization of high AC activity. Warmer colors represent higher ratios (left). Overlay of actin (red) and active Cofilin (green) shows that the highest Cofilin activity (arrowhead) is at the base of filopodia (right). Scale bar represents 3 μm.

(G) Quantification of filopodia number per cell shows a decrease in *AC KO* neurons compared to wild-type neurons. The results are from three experiments, $n \geq 120$ cells for each group.

(H) Quantification of fascin/radial actin colocalization shows decreased Fascin-positive actin bundles in *AC KO* neurons compared to wild-type neurons. $n \geq 75$ cells from three experiments.

(I) Mena localization to the leading edge cell membrane is disrupted in the *AC KO* neurons. The fluorescent micrographs show Mena-mCherry expression patterns in stage 1 wild-type and *AC KO* neurons. Mena localizes to the edge of extending protrusions (white arrowheads). In *AC KO*s, Mena is dispersed throughout the cell and accumulates in punctae away from the leading edge (white arrowheads). Scale bar represents 3 μm.

(J) Quantification of the percentage of cells with leading edge Mena localization in stage 1 wild-type and *AC KO* neurons. The results are from three experiments, $n \geq 80$ cells for each group.

(K) Fluorescent images of F-actin (phalloidin) and kabiramide (barbed ends) in stage 1 wild-type and *AC KO* neurons. The right panels are magnified views of the indicated regions. Arrowheads indicate leading edge in wild-type. Scale bar represents 10 μm.

(L) Quantification of the percentage of cells with leading edge kabiramide localization in stage 1 wild-type and *AC KO* neurons. The results are from three experiments, $n \geq 150$ cells for each group.

*$p < 0.05$, **$p < 0.01$, ***$p < 0.001$. Error bars represent SD.

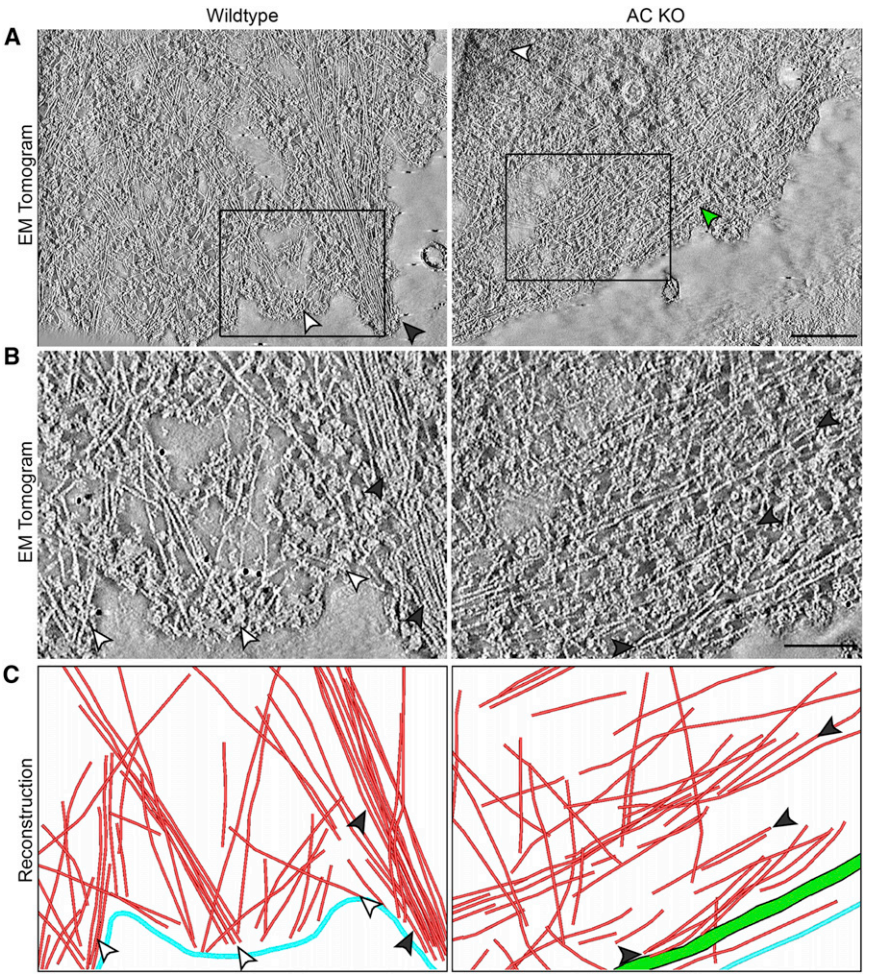

Figure 4. Ultrastructural Aberrations in the Cytoskeleton of Stage 1 ADF/Cofilin Knockout Neurons

(A) Single frames of electron tomograms showing the ultrastructure of the cytoskeleton of wild-type and *AC KO* neurons. In wild-type neurons, radially oriented actin filaments are organized in loose networks in lamellipodial regions (white arrowhead) and in tight bundles in filopodia (black arrowhead). The *AC KO* neuron has a denser, disorganized actin network. Extremely dense F-actin causes distortions in the tomograms (white arrowhead). Looping microtubules are seen along the cell edge (green arrowhead). Scale bar represents 200 nm. See also Movies S2 and S3.

(B) Magnified view of the regions indicated in (A). The arrangement of individual actin filaments are observed in filopodia (black arrowheads) and lamellipodia (white arrowheads). In the *AC KO* neuron, dense, circumferentially oriented actin filaments are apparent (black arrowheads). Scale bar represents 100 nm.

(C) Reconstruction of actin filaments (red) and microtubule (green) with respect to cell edge (blue) from tomograms of regions shown in (B).

nucleation can occur at the appropriate location in the absence of AC.

High-resolution electron microscopy tomography revealed that in wild-type stage 1 neurons, actin filaments were radially oriented in tight bundles in filopodia or in a meshwork of filaments largely oriented toward the cell edge of lamellipodial veils (Figures 4A–4C, Movie S2). In contrast, *AC KO* neurons had a disorganized dense actin filament network with a large population of individual filaments oriented circumferentially, parallel to the cell edge. Furthermore, there was no actin bundling observed in *AC KO* neurons (Figures 4A–4C, Movie S3). Thus, AC proteins not only regulate the F-actin quantity, but also the configuration of the neuronal actin network.

ADF/Cofilin Proteins Are Essential for Retrograde F-Actin Flow and Actin Turnover

The increased levels of F-actin and disordered filaments in *AC KO* neurons suggested a defect in actin turnover. Therefore, we examined actin dynamics by live-cell imaging using Lifeact-GFP. Stage 1 wild-type neurons had a very dynamic actin network, forming and retracting filopodia within minutes (Figure 5A, Movie S4). In contrast, *AC KO* neurons had an immobile actin network (Figure 5B, Movie S4). Kymograph analysis showed that while wild-type neurons had an average retrograde flow rate of 4.46 ± 0.97 μm/min, *AC KO* neurons had an average rate of 0.14 ± 0.4 μm/min, a more than 30-fold reduction ($p < 0.001$; Figures 5A–5C). There was a similar reduction in protrusion frequency and distance in *AC KO* neurons compared to wild-type neurons (Figures 5D and 5E). Consistently, photobleaching GFP-actin in the peripheral actin network of *AC KO* neurons showed an over 40-fold higher half-fluorescence recovery ($t_{1/2}$) compared to wild-type neurons (Figures 5F and 5G).

Having found such severe changes in actin organization and dynamics, we wanted to test whether *AC KO* cells could recover and form normal actin structures. To this end, we altered Cofilin expression levels in a temporally controlled manner by fusing Cofilin to a destabilization domain (DD), which targets proteins for rapid proteasome-mediated degradation (Banaszynski et al., 2006). Addition of shield reagent protected Cofilin-DD from degradation and led to detectable Cofilin expression within 2 hr and high expression by 8 hr (Figures 5H and S4B). *AC KO* neurons expressing DD remained quiescent and did not show changes in actin structure or dynamics (data not shown). Within 6 hr after Cofilin-DD stabilization with shield reagent, *AC KO* neurons showed some radially oriented actin filament bundles (Figure 5I). After 10–12 hr, *AC KO* neurons formed prominent circumferential actin and filopodia and showed increased actin retrograde flow resembling wild-type neurons (Figure 5I, Movie S5). In accord with this, after shield addition, Fascin-GFP reoriented into peripheral actin bundles and VASP-GFP repositioned to the leading edge (data not shown). These data

show that the profoundly disorganized actin network in *AC KO* neurons can be structured by simply bringing Cofilin back into the system. AC is thus vital for actin organization and retrograde flow.

Actin Destabilization Restores Neurite Formation in *AC KO* Neurons

During neuritogenesis, microtubules extend in bundles out of the neuronal sphere to form the backbone of neurites. We hypothesized that the drastic disorganization of F-actin structure in *AC KO* neurons affects the microtubule organization necessary to form neurites. Indeed, in *AC KO* neurons, immunocytochemistry showed that single microtubules splayed out in an irregular fashion and looped at the cell edge (data not shown), reminiscent of the microtubules in neurons treated with 10 nM jasplakinolide (Figure 1G). In live-cell imaging experiments, EB3-mCherry-labeled microtubules grew out radially from the soma into the actin-rich periphery often along F-actin bundles, where they slowed down, paused, and even exhibited retrograde displacements (Figures 6A–6F, Movie S6). As a result, microtubule advance was 46% faster in the soma compared to the actin-rich periphery in wild-type neurons (0.32 ± 0.04 μm/s in the soma versus 0.21 ± 0.01 μm/s in the periphery, $p < 0.001$; Figure 6B). In *AC KO* neurons, EB3-mCherry-tagged microtubules grew out in a radial fashion from the soma into the periphery but were laterally displaced at the edge of the neuron, resulting in an increased percentage of cells with looping microtubules (Figures 6E and 6F, Movie S6). Throughout all regions of *AC KO* neurons, microtubules advanced at slower, but constant, velocities compared to wild-type neurons (0.22 ± 0.04 μm/s in the *AC KO* soma, $p < 0.001$; Figures 6A and 6B) and largely avoided the F-actin network (Figures 6A–6E). Importantly, upon latrunculin B-induced depolymerization of the actin cytoskeleton, microtubule growth increased both in the peripheral zone of wild-type neurons and in all regions of *AC KO* neurons and resembled the growth pattern observed in the soma of wild-type neurons, which is devoid of actin filaments (Figures 6C and 6D).

Moreover, after actin depolymerization with latrunculin B treatment in *AC KO* neurons, EB3 comets emerged from the cell soma and grew in bundles into nascent neurites within 2–3 hr (Figure 6G). After 1 day, latrunculin B, cytochalasin D, or the actin-severing drug swinholide increased neuritogenesis in *AC KO* neurons 2-fold to 4-fold (Figures 6H and 6I). The protrusion of microtubules is essential for neurite formation as low levels of the microtubule-destabilizing drug nocodazole attenuated the neurite-restoring effects of cytochalasin D and latrunculin B (Figure S5). Instead, manipulations that were targeted either to stimulate integrin signaling or to bundle actin filaments, which restore neurite formation in *Mena/VASP/EVL KO* neurons (Dent et al., 2007), did not enable neurite formation in *AC KO* neurons (Figure S6). We conclude that the drastic F-actin disorganization in *AC KO* neurons obstructs intracellular space and misdirects microtubule growth patterns. Furthermore, a pharmacological depolymerizing activity bypasses the need for AC proteins, allowing microtubules to coalesce and to radially protrude to generate neurites.

The Severing Activity of AC Proteins Regulates Neurite Formation

Although in some instances the function of ADF and Cofilin are overlapping (Hotulainen et al., 2005), ADF depolymerizes actin filaments better than Cofilin, whereas Cofilin severs filaments better than ADF (Bernstein and Bamburg, 2010). Therefore, we determined the individual contributions of ADF and Cofilin to neuritogenesis. First, we examined the development of neurons with either monoallele *ADF* expression (*NesCre*$^{+/-}$, *ADF*$^{+/-}$, *cofilin*$^{flox/flox}$) or monoallele cofilin expression (*NesCre*$^{+/-}$, *ADF*$^{-/-}$, *cofilin*$^{flox/+}$). *ADF* monoallele expression resulted in defective neuritogenesis with a significant increase in the percentage of cells in stage 1 (Figures S7A and S7B). In contrast, *cofilin* monoallele expression conferred wild-type-like neuronal development, with the majority of neurons in stage 2 or stage 3 (Figures S7C and S7D).

Consistently, reintroduction of ADF into *AC KO* neurons only partially restored neurite formation in *AC KO* neurons, whereas Cofilin reintroduction almost completely reversed the neuritogenesis defect, resulting in cells with wild-type morphology in cell culture (Figures 7A and 7B). Moreover, Cofilin re-expression restored normal neuronal development in *AC KO* cortical slices (Figures 7C, 7D, and S7E). Analysis of the F-actin organization revealed that both ADF and Cofilin restored the gross organization of actin architecture. The percentage of cells extending filopodia increased 2-fold in ADF or Cofilin-transfected *AC KO* neurons (Figures 7E and 7F). However, kymograph analysis of live-cell imaging of *AC KO* neurons cotransfected with Lifeact-GFP revealed that only Cofilin expression increased actin retrograde flow to 4.0 ± 1.0 μm/min, nearly a complete rescue, while ADF only partially increased actin retrograde flow to 2.9 ± 1.2 μm/min, a 65% rescue (Figures 7E and 7G). Thus, while ADF and Cofilin are equally adept at stimulating filopodia formation, Cofilin has a higher propensity for driving actin retrograde flow and neuritogenesis.

We next asked whether the increased aptitude for F-actin severing underlies the increased effectiveness of Cofilin for facilitating actin retrograde flow and neuritogenesis. Biochemical studies have shown that when Tyr82 is mutated to Phe (Y82F), Cofilin loses its depolymerizing activity but retains its severing activity (Moriyama and Yahara, 1999, 2002). Conversely, when Ser94 is mutated to Asp (S94D), Cofilin loses its severing activity but retains its depolymerizing activity. The introduction of the nonsevering mutant CofS94D-RFP did not greatly alter actin organization and dynamics in *AC KO* neurons, leading only to a slight increase in filopodia (Figures 8A–8E) and in actin retrograde flow (Figures 8A and 8B, Movie S7). However, the expression of the nondepolymerizing mutant CofY82F-RFP, which only can sever actin filaments, restored the prototypical actin architecture in *AC KO* neurons, including the percentage of cells with filopodia (Figures 8A–8E), and substantially increased actin retrograde flow to over 50% of wild-type levels (Figures 8A and 8B, Movie S7). Concomitantly, CofY82F restored neuritogenesis in *AC KO* neurons by over 2-fold, while CofS94D only marginally increased neurite formation in *AC KO* neurons (Figures 8C and 8D). Taken together, these data show that the transformation from simple spherical cells into morphologically distinct,

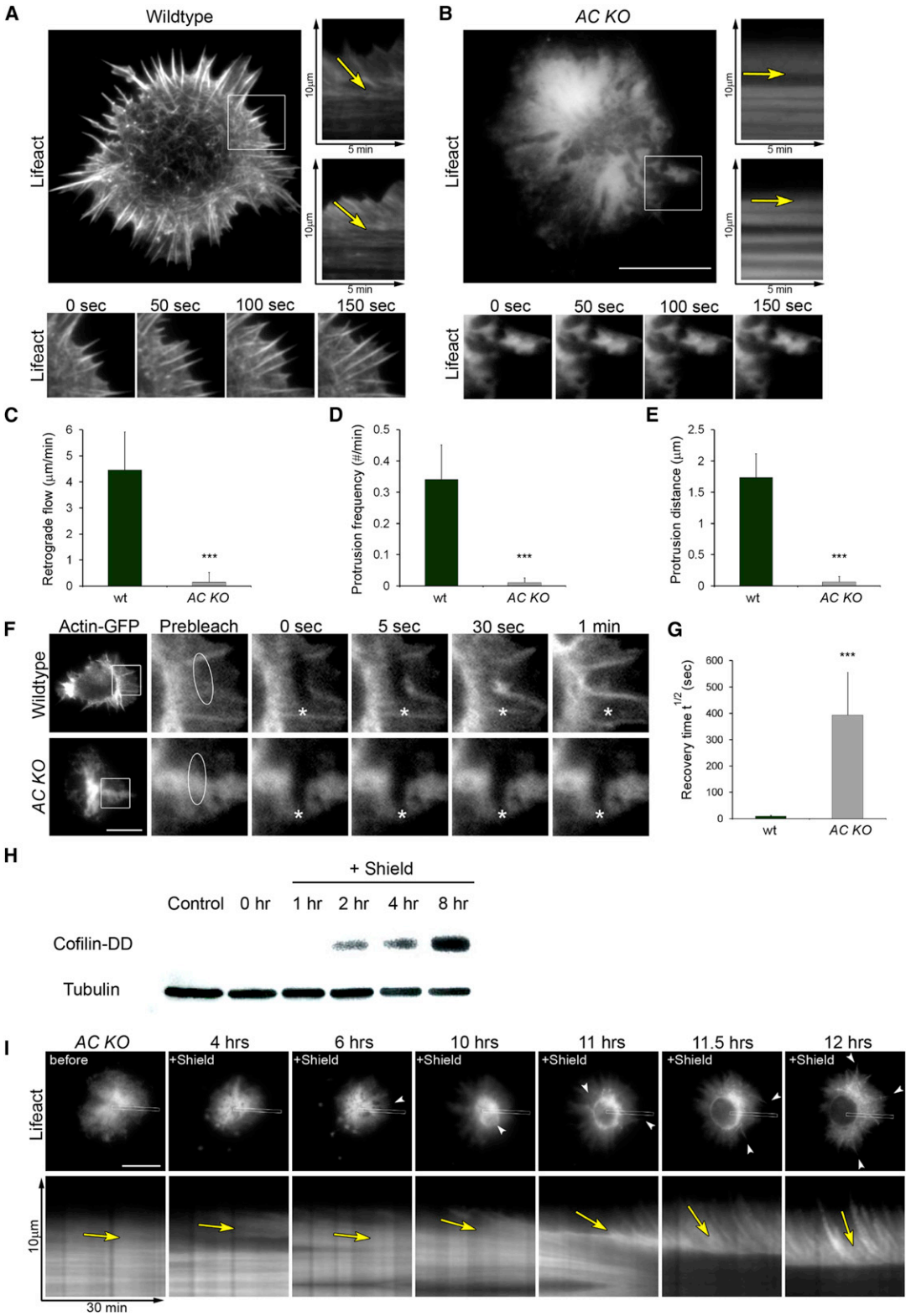

Figure 5. ADF/Cofilin Is Essential for Actin Retrograde Flow in Neurons

(A) Single frame from live-cell imaging series of a wild-type neuron expressing Lifeact-GFP. The kymographs show actin retrograde flow from two line scans. Yellow arrows highlight actin translocation. The bottom panels show normal filopodial dynamics in the boxed region from the top panel. See also Movie S4.

(legend continued on next page)

elaborate neurons relies on actin retrograde flow driven by the severing activity of AC proteins.

DISCUSSION

Our study revealed that ADF/Cofilin drives actin retrograde flow and regulates neurite formation. The mechanism underlying neuritogenesis entails dynamizing and restructuring F-actin, which maneuvers radial microtubule advance and bundling. Specifically, the severing activity of AC proteins is a key stimulant for the actin organization and retrograde flow necessary for neuritogenesis. Together, our data define a fundamental role for ADF/Cofilin during neuritogenesis and advance our knowledge on how neurons break the neuronal sphere.

ADF/Cofilin Regulates Actin Retrograde Flow

From migrating cells to neuronal growth cones, actin retrograde flow is an essential component in cell motility (Dent et al., 2011; Lowery and Van Vactor, 2009; Small and Resch, 2005). It consists of actin subunit integration at the plus end of actin filaments at the leading edge and retrograde movement of the filaments and their depolymerization at the minus end. However, its precise role in regulating neuritogenesis is still unclear. Moreover, inhibition of actin-binding proteins that are thought to be involved in retrograde flow, including myosin II, Arp 2/3, and Ena/VASP, only moderately reduces actin retrograde flow in neurons (Dent et al., 2007; Korobova and Svitkina, 2008; Medeiros et al., 2006), indicating that key factors have remained unidentified.

Here, we identified AC as a key player regulating actin retrograde flow. Consistently, in vitro studies revealed that the minimal requirements for actin turnover rates reflecting the in vivo kinetics are AC proteins together with capping protein and formin (Michelot et al., 2007), while motor proteins or actin crosslinking proteins are not needed. Similarly, AC proteins, capping protein, and Arp2/3 are sufficient to recapitulate Listeria motility in vitro (Loisel et al., 1999).

How do AC proteins help to drive actin retrograde flow and organization? And how does this influence neurite formation (Figures 8F and 8G)? The location of actin polymerization is tightly regulated, occurring nearly exclusively at the leading edge of growth cones (Forscher and Smith, 1988), probably due to the linkage of actin nucleators to the membrane (Pak et al., 2008; Saarikangas et al., 2010). As they grow, actin filaments (Figure 8F, red) undergo molecular aging, so that the original ATP-actin (light red subunits) becomes ADP-actin (dark red subunits) over time and at locations distant from the membrane. Since AC proteins (yellow spheres) bind preferentially to this older, ADP-actin portion of filaments, actin depolymerization, severing (Pac-Man), turnover and reorganization, is promoted away from the leading edge. Indeed, we found that active AC is positioned at the base of filopodia and lamellipodia, ideally poised for dismantling F-actin. In the absence of AC proteins, attenuated actin disassembly may lead to the congestion of the intracellular space with actin filaments that reorient haphazardly in response to the pressure of polymerization. Hence, AC may regulate actin organization simply by virtue of its primary activity: increasing actin turnover. Consistent with this view, the reintroduction of Cofilin function restored retrograde flow and reorganized actin superstructures.

Our data further show that actin retrograde flow is driven by Cofilin's propensity for F-actin severing. These data are consistent with current actin turnover modeling, which indicates that the most effective way to achieve accelerated actin retrograde flow would be to enhance actin deconstruction at the minus end of filaments (Roland et al., 2008).

ADF/Cofilin Render the Actin Cytoskeleton Permissive for Microtubules to Form a Neurite

Filopodia have recently been linked to neuritogenesis as they engorge with microtubules and elongate into nascent neurites (Dent et al., 2007). From this work and our own results, it is plausible that these radial actin bundles are the sites where microtubules can extend into the peripheral zone in the correct, radial orientation, which is necessary for the consolidation and advance of a nascent neurite (Figure 8F). *AC* knockout neurons displayed a marked decrease in radially oriented actin filaments in lamellipodia and filopodia while concomitantly exhibiting abnormal microtubule growth patterns and looping trajectories. Thus, the lack of this permissive actin platform for microtubules to grow along may underlie the failure of neuritogenesis in *AC KO* neurons. However, neuritogenesis is also attenuated in situations where filopodia appear normal, such as in *ADF* monoallele neurons and wild-type neurons treated with low levels of jasplakinolide. Thus, actin dynamics is also important for this process. One possibility is that a dense

(B) Single frame of a live-cell imaging series of an *AC KO* neuron. The kymographs show actin retrograde flow from two line scans. The yellow arrows indicate the lack of translocation of actin filaments. The bottom panels show a lack of filopodial dynamics in the boxed region from the top panel. See also Movie S4. Scale bar represents 10 μm.
(C) Quantification of actin retrograde flow in wild-type and *AC KO* neurons; $n \geq 20$ cells from three experiments.
(D) Quantification of protrusion frequency in wild-type and *AC KO* neurons; $n \geq 20$ cells from three experiments.
(E) Quantification of protrusion distance in wild-type and *AC KO* neurons; $n \geq 20$ cells from three experiments.
(F) Fluorescent recovery after photobleaching (FRAP) reveals that *AC KO* neurons have strikingly reduced actin turnover. Single frames of neurons expressing GFP-actin are shown. Asterisks show original photobleached site. Scale bar represents 10 μm.
(G) Quantification of fluorescent recovery in wild-type and *AC KO* neurons; numbers are averages of $n \geq 20$ cells.
(H) Western blot of hippocampal neurons expressing DD alone (control) or Cofilin-DD. Time after shield addition is indicated. After shield addition, there is an increase in Cofilin-DD expression 2–8 hr as detected with an antibody to DD.
(I) Reactivation of Cofilin-DD by addition of shield reagent restores actin organization and dynamics in *AC KO* neurons expressing Lifeact-GFP and Cofilin-DD. Kymographs of line scans from the indicated region of the neuron show actin retrograde flow (yellow arrows). Subtle changes in the actin occur after 6 hr and more drastic reorganization of the actin network and increased actin retrograde flow occurs at 10–12 hr. See also Movie S5. Scale bar represents 10 μm.
***$p < 0.001$. Error bars represent SD.

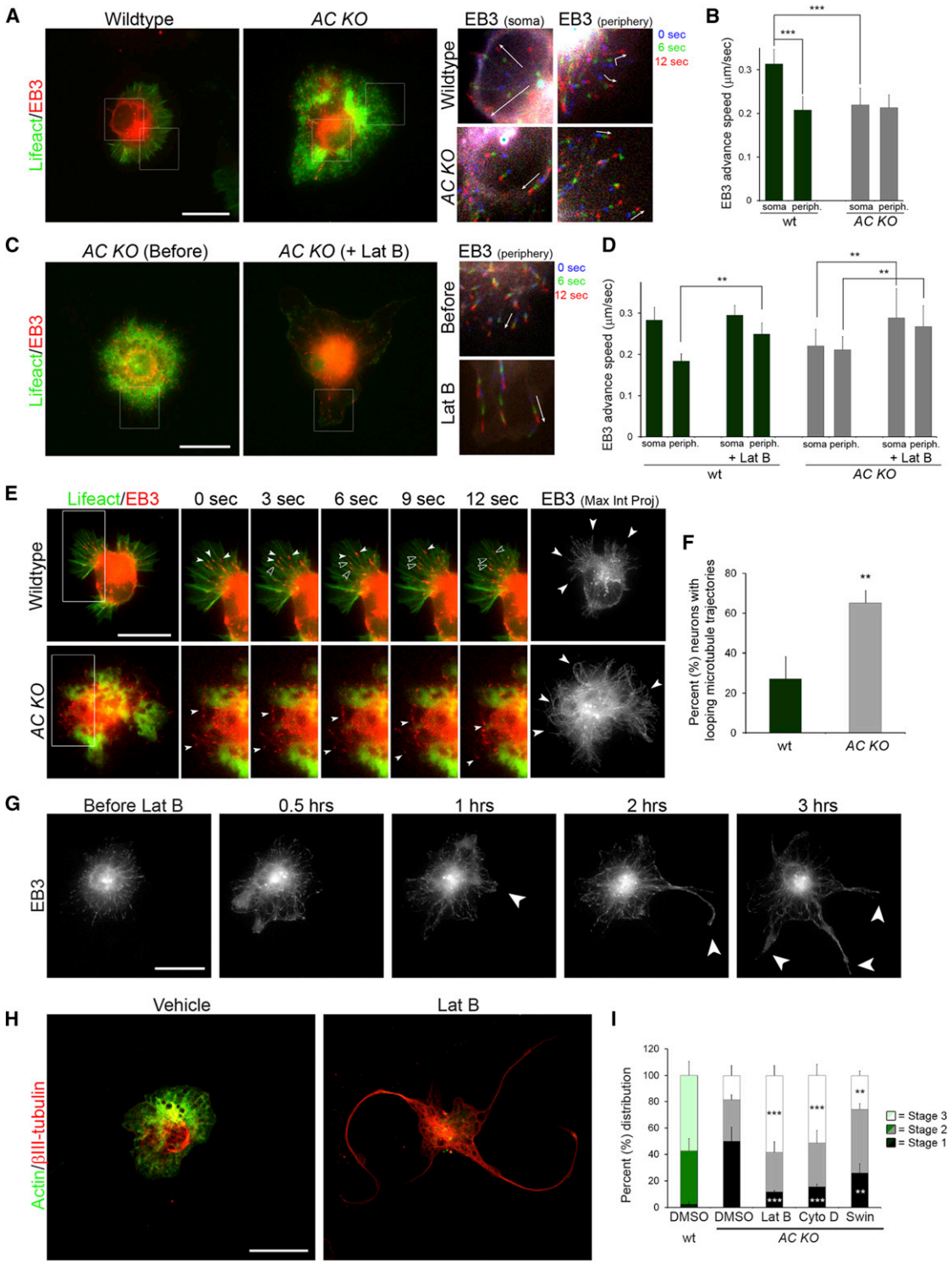

Figure 6. Actin Destabilization Permits Radial Microtubule Growth and Restores Neurite Formation in *AC KO* Neurons

(A) Microtubule advance is slower in *AC KO* neurons. Single frames are shown from live-cell imaging series of neurons expressing Lifeact-GFP and EB3-mCherry (left). Color-coded projections of EB3 over time are shown (right). White arrows indicate movement of EB3. EB3-mCherry velocities are slower in the periphery of WT cells compared to the soma. *AC KO* neurons display constant but slower EB3 advance speeds in both regions of the cells. Scale bar represents 10 μm.

(B) Quantification of the advance rates of EB3-mCherry in the soma and actin-rich periphery of WT and *AC KO* neurons. n ≥ 15 cells.

(legend continued on next page)

actin network simply prevents microtubules to bundle and to protrude. In this view, microtubules may grow along radial F-actin bundles and filopodia because they offer the path of least resistance in the retrogradely flowing actin network. Since there is less interweaving of actin fibers in radial actin bundles compared to the actin network in regions of lamellipodia and proximal actin arcs, microtubules can grow in an unimpeded fashion. Indeed, analysis of microinjected fluorescent particles of different molecular weights showed that the actin network in cells can be dense enough to prevent the movement of structures having the size of microtubules (Luby-Phelps and Taylor, 1988). Consistent with this idea, the pharmacological destabilization of actin filaments in *AC KO* neurons restored neuritogenesis. Furthermore, it also allowed the proper orientation and growth of microtubules, enabling them to protrude through the cell rim to induce a neurite. Thus, our data suggest that during neuritogenesis, AC proteins enable microtubule protrusion both by dismantling dense actin structures to free intracellular space and by helping organize parallel F-actin bundles that facilitate radial microtubule growth and bundling (Figure 8F). In the absence of AC proteins, the congestion and lack of ''permissive'' F-actin bundles obstructs directed microtubule protrusion, ultimately leading to a failure of neuritogenesis (Figure 8G).

ADF/Cofilin and Brain Development

Our study shows that the effects of AC-mediated actin dynamics on early brain development are of paramount importance and relevant for human brain development. For example, the neurocognitive disorder Smith-Lemli-Optiz syndrome has recently been linked to neurite growth defects rooted, perhaps, in a misregulation of Cofilin activity (Jiang et al., 2010). Furthermore, the cortical ectopias we observed in embryonic *AC KO* brains resemble the cobblestone cortex of mouse models of type II lissencephaly (Bielas et al., 2004). Our study, along with others, highlights the importance of exploring the role of cytoskeleton-mediated mechanisms in human brain disorders (Heng et al., 2010). We therefore see the further elucidation of the mechanism of microtubule-actin interactions and the involved players during neurite growth as essential to future studies in understanding brain development and pathology.

EXPERIMENTAL PROCEDURES

Transgenic Mice

Conditional ablation of ADF/Cofilin proteins in the nervous system was achieved by crossing mice with genomic *ADF* ablation and expressing *Cofilin floxed* alleles (*ADF*$^{-/-}$, *cofilin*$^{flox/flox}$) (Bellenchi et al., 2007) with mice lines expressing *Cre recombinase* (*Cre*) from the nervous system-specific promoters (see Supplemental Experimental Procedures for details).

Histological Analysis

The heads of E17 mouse embryos were fixed in 4% paraformaldehyde, 4% sucrose in PBS or PHEM buffer and prepared for cryosectioning using standard procedures (Tahirovic et al., 2010).

In Utero Electroporation

In utero electroporation experiments were performed essentially as described (Saito, 2006) but optimized to achieve moderate expression of transgenes in cortical neurons.

Cortical Slice Culture and Adenovirus Transduction

Acute organotypic cortical slice culture experiments were performed essentially as described (Flynn et al., 2009). We added 10^6–10^7 pfu of Cofilin-RFP or RFP control adenovirus directly on the brain tissue at 24 hr and the tissue was fixed and stained at 72 hr.

Neuronal Cell Culture

Primary mouse hippocampal and cortical neurons were dissected from E16.5–E17 brains and cultured as previously described (Garvalov et al., 2007).

Live-Cell Microscopy

The DeltaVision RT (Applied Precision) setup was primarily used for live-cell imaging of fluorescent proteins. Neurons from Lifeact-GFP transgenic mice (Riedl et al., 2010) were used to visualize actin dynamics. In other experiments, *AC KO* neurons or wild-type littermate controls were transfected with Lifeact-GFP and/or EB3-mCherry to label the actin and growing microtubules, respectively. Rescue experiments with Cofilin-DD were performed on AC KO neurons cotransfected with Lifeact-GFP and pTuner Cofilin-DD or empty pTuner plasmid (Clontech).

Immunocytochemistry

Indirect immunofluorescence was performed under conditions optimal for the preservation of the cytoskeleton. Neuronal cultures were fixed with 4% paraformaldehyde, 4% sucrose in PHEM fixation buffer and prepared for immunofluorescence (Witte et al., 2008).

Local Actin Destabilization and Neurite Formation

Local actin destabilization was achieved by application of a local field of latrunculin B essentially as described (Bradke and Dotti, 1999).

(C) Actin depolymerization by latrunculin B (Lat B) increases microtubule advance velocities. Single frames are shown from live-cell imaging series of neurons expressing Lifeact-GFP and EB3-mCherry (left). Color-coded projections of EB3 before and after Lat B treatment over time are shown (right). White arrows indicate movement of EB3. EB3-mCherry velocities are faster after actin depolymerization. Scale bar represents 10 μm.
(D) Quantification of the advance rates of EB3-mCherry before and after latrunculin B treatment. n ≥ 15 cells.
(E) The growing ends of microtubules have increased looping trajectories in *AC KO* neurons. Single frames of neurons expressing EB3-mCherry and Lifeact-GFP and maximum intensity projections of the different time points of EB3 over a 2 min time period are shown. Solid white arrowheads indicate anterograde movement of EB3. The open arrowheads indicate when EB3 comets pause or move in a retrograde manner. See also Movie S6. Scale bar represents 10 μm.
(F) Quantification of cells with looping microtubules. n ≥ 45 cells from three experiments.
(G) Actin destabilization rescues neuritogenesis in *AC KO* neurons. Images EB3-mCherry from a live-cell imaging experiment of an *AC KO* neuron treated with latrunculin B (Lat B). Arrowheads indicate sites of EB3 comets in growing neurites. Scale bar represents 20 μm.
(H) Actin destabilization with Lat B leads to radial microtubule growth and the formation of neurites. Actin and βIII-tubulin staining is shown for *AC KO* neurons at 2 DIV. Scale bar represents 20 μm.
(I) Quantification of neuronal development stages in DMSO-, Lat B-, cytochalasin D (Cyto D)-, and swinholide (Swin)-treated cultures. n ≥ 200 cells from three experiments at 2 DIV.
**$p < 0.01$, ***$p < 0.001$. Error bars represent SD.

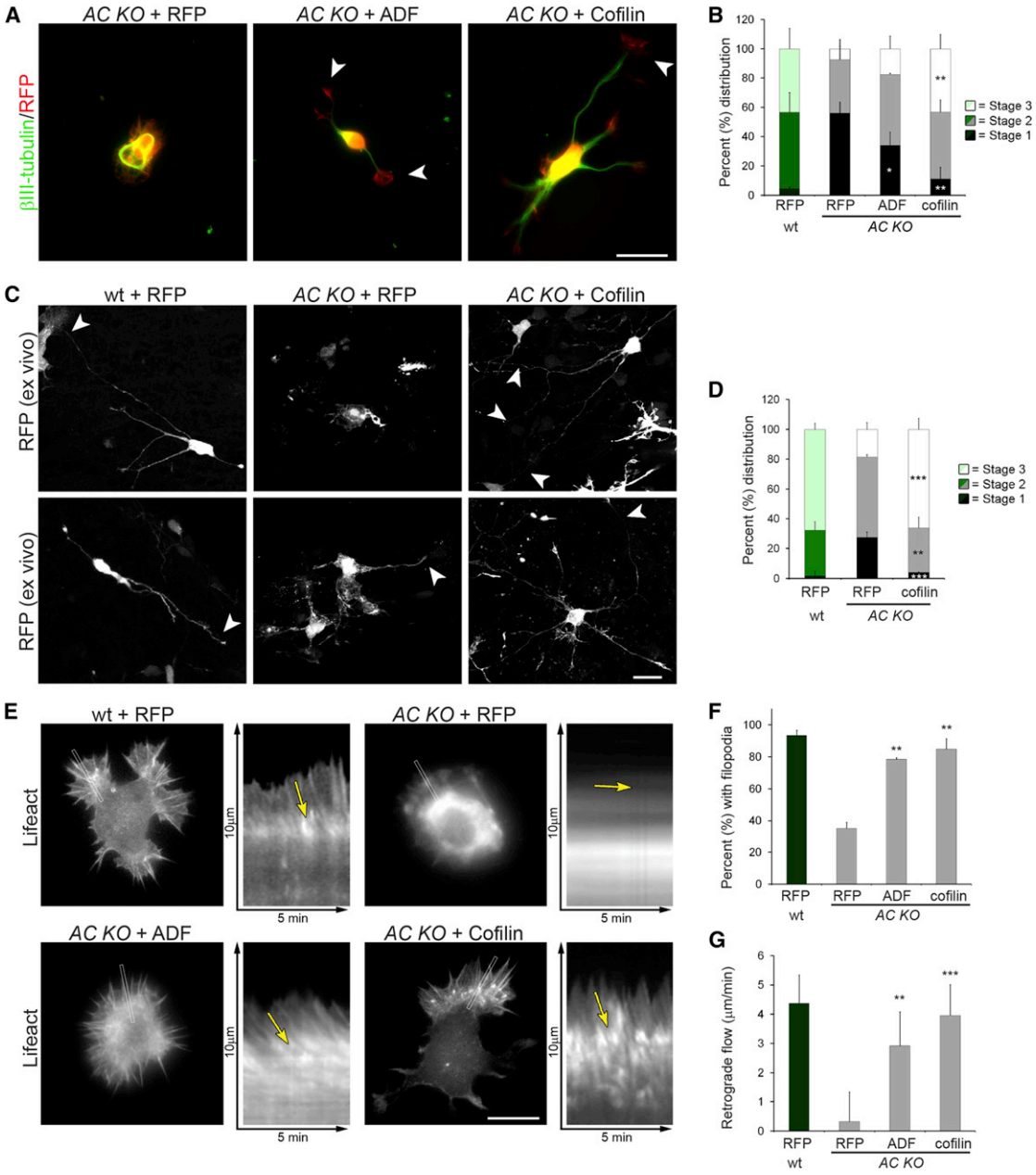

Figure 7. Cofilin Re-expression in AC KO Neurons Rescues Neuritogenesis, Filopodia Formation, and Actin Retrograde Flow

(A) Micrographs of RFP and βIII-tubulin staining in *AC KO* neurons at 2 DIV. Arrowheads indicate growth cones of neurites with ADF or Cofilin expression. Scale bar represents 20 μm.

(B) Quantification of the developmental stages in wild-type + RFP-, *AC KO* + RFP-, *AC KO* + ADF-RFP-, and *AC KO* + cof-RFP-expressing neurons. n ≥ 100 cells from three experiments at 2 DIV.

(C) Maximum intensity projections of RFP signal of wild-type and *AC KO* neurons in cortical tissue slices. Arrowheads indicate neurites. Scale bar represents 20 μm.

(D) Quantification of the developmental stages in wild-type + RFP-, *AC KO* + RFP-, and *AC KO* + cof-RFP-expressing neurons. n ≥ 100 cells from three experiments at 2 DIV.

(E) Actin retrograde flow is restored by re-expression of Cofilin and, to a lesser extent, of ADF. Single frames are shown of Lifeact-GFP from live-cell imaging series of a control wild-type neuron (RFP), a control *AC KO* neuron (RFP), an ADF-RFP-expressing *AC KO* neuron, and a Cofilin-RFP-expressing *AC KO* neuron. Kymographs of the indicated line scans show the retrograde actin flow. The yellow arrows indicate the translocation of F-actin. Scale bar represents 10 μm.

(F) Quantification of the percentage of cells with filopodia in stage 1 neurons is shown. n ≥ 95 cells from three experiments.

(G) Quantification of actin retrograde flow in wild-type, *AC KO* control, *AC KO* + ADF, and *AC KO* + Cofilin neurons; n ≥ 20 cells for each condition.

*p < 0.05, **p < 0.01, ***p < 0.001. Error bars represent SD.

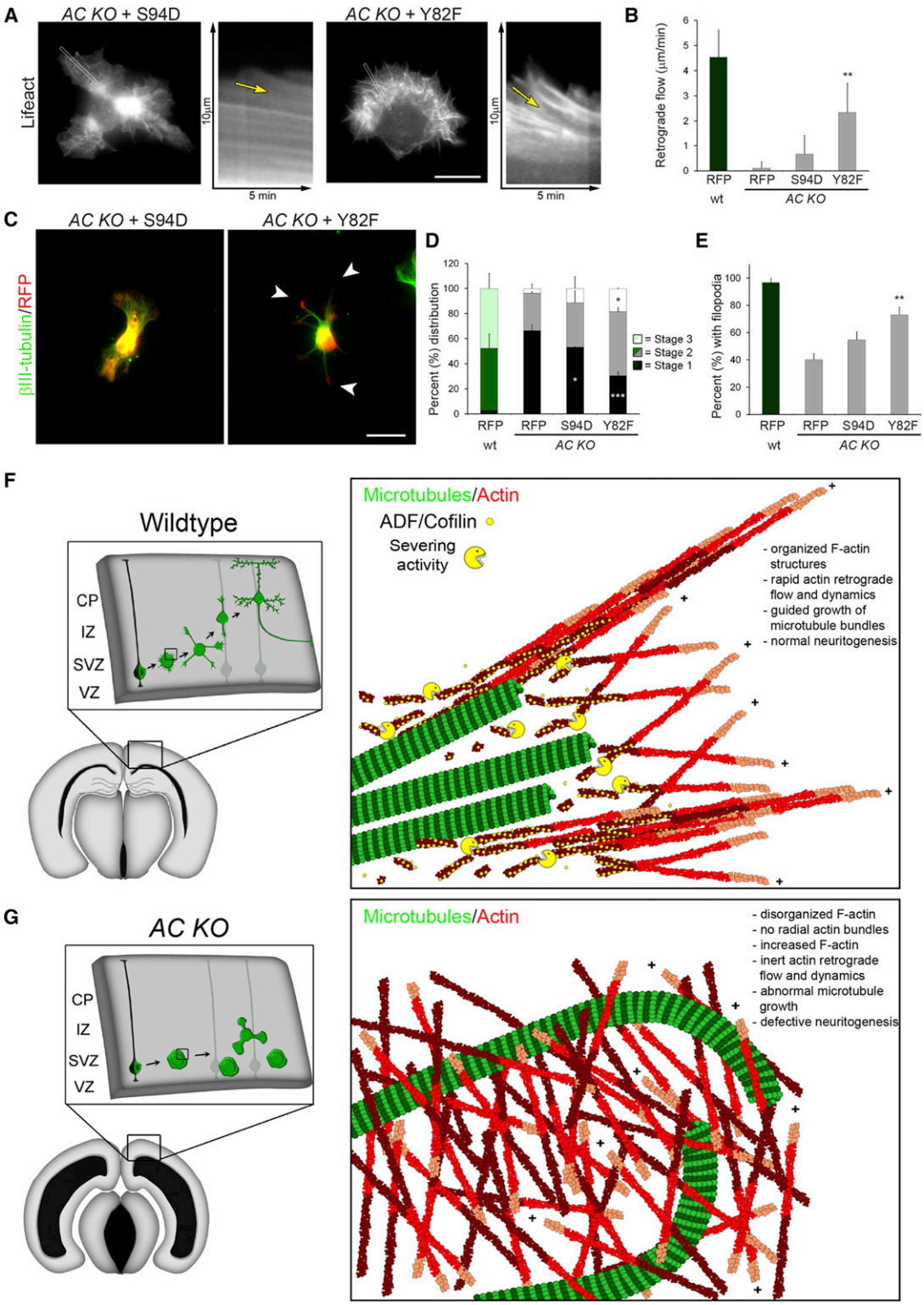

Figure 8. The Severing Activity of Cofilin Is More Important than Its Depolymerizing Activity and a Model of the Effects of AC Activity on Actin and Microtubules during Neurite Formation

(A) Retrograde actin flow is moderately rescued by expression of CofY82F. Single frames are shown of Lifeact-GFP from live-cell imaging series of a CofS94D-RFP-expressing neuron and a CofY82F-RFP-expressing neuron. Kymographs of line scans show retrograde actin flow. The yellow arrows follow the translocation of F-actin. See also Movie S7. Scale bar represents 10 μm.

(legend continued on next page)

Electron Microscopy

The ultrastructural analysis of the actin cytoskeleton was essentially performed as described (Auinger and Small, 2008) with minor modifications for optimal preservation of the neuronal cytoskeleton.

Protein Analysis

The cortices of E16.5–E18 embryonic brains were rapidly dissected and resuspended in SDS lysis buffer and prepared for SDS-PAGE and western blotting. Relative levels of filamentous and globular actin were determined using the F:G actin kit from Cytoskeleton according to the manufacturer's guidelines.

SUPPLEMENTAL INFORMATION

Supplemental Information includes seven figures, Supplemental Experimental Procedures, and seven movies and can be found with this article online at http://dx.doi.org/10.1016/j.neuron.2012.09.038.

ACKNOWLEDGMENTS

We are very grateful for the technical assistance of Ralf Zenke, Ireen König, and Hans Fried. Frank Gertler, Franck Polleux, and Gerard Marriott receive our appreciation for reagents supplied in this study. We thank Barbara Bernstein, Mark Hübener, Artur Kania, Claudia Laskowski, Klemens Rottner, Michael Sixt, and Michael Stiess for helpful comments and suggestions on the manuscript. Xiao-bing Yuan (Shanghai Institute for Biological Sciences) is gratefully acknowledged for instruction in utero electroporation techniques. We gratefully acknowledge support from the Marie Curie Actions (K.C.F.), the Max Planck Society (F.B), the Deutsche Forschungsgemeinschaft (F.B. and W.W.), and Austrian Science Fund (FWF to J.V.S.).

Accepted: September 25, 2012
Published: December 19, 2012

REFERENCES

Akhmanova, A., and Steinmetz, M.O. (2008). Tracking the ends: a dynamic protein network controls the fate of microtubule tips. Nat. Rev. Mol. Cell Biol. *9*, 309–322.

Andrianantoandro, E., and Pollard, T.D. (2006). Mechanism of actin filament turnover by severing and nucleation at different concentrations of ADF/cofilin. Mol. Cell *24*, 13–23.

Arimura, N., and Kaibuchi, K. (2007). Neuronal polarity: from extracellular signals to intracellular mechanisms. Nat. Rev. Neurosci. *8*, 194–205.

Auinger, S., and Small, J.V. (2008). Correlated light and electron microscopy of the cytoskeleton. Methods Cell Biol. *88*, 257–272.

Banaszynski, L.A., Chen, L.C., Maynard-Smith, L.A., Ooi, A.G., and Wandless, T.J. (2006). A rapid, reversible, and tunable method to regulate protein function in living cells using synthetic small molecules. Cell *126*, 995–1004.

Barnes, A.P., and Polleux, F. (2009). Establishment of axon-dendrite polarity in developing neurons. Annu. Rev. Neurosci. *32*, 347–381.

Bear, J.E., and Gertler, F.B. (2009). Ena/VASP: towards resolving a pointed controversy at the barbed end. J. Cell Sci. *122*, 1947–1953.

Bellenchi, G.C., Gurniak, C.B., Perlas, E., Middei, S., Ammassari-Teule, M., and Witke, W. (2007). N-cofilin is associated with neuronal migration disorders and cell cycle control in the cerebral cortex. Genes Dev. *21*, 2347–2357.

Bernstein, B.W., and Bamburg, J.R. (2010). ADF/cofilin: a functional node in cell biology. Trends Cell Biol. *20*, 187–195.

Bielas, S., Higginbotham, H., Koizumi, H., Tanaka, T., and Gleeson, J.G. (2004). Cortical neuronal migration mutants suggest separate but intersecting pathways. Annu. Rev. Cell Dev. Biol. *20*, 593–618.

Bradke, F., and Dotti, C.G. (1999). The role of local actin instability in axon formation. Science *283*, 1931–1934.

Carlier, M.F., Laurent, V., Santolini, J., Melki, R., Didry, D., Xia, G.X., Hong, Y., Chua, N.H., and Pantaloni, D. (1997). Actin depolymerizing factor (ADF/cofilin) enhances the rate of filament turnover: implication in actin-based motility. J. Cell Biol. *136*, 1307–1322.

Cohan, C.S., Welnhofer, E.A., Zhao, L., Matsumura, F., and Yamashiro, S. (2001). Role of the actin bundling protein fascin in growth cone morphogenesis: localization in filopodia and lamellipodia. Cell Motil. Cytoskeleton *48*, 109–120.

Conde, C., and Cáceres, A. (2009). Microtubule assembly, organization and dynamics in axons and dendrites. Nat. Rev. Neurosci. *10*, 319–332.

da Silva, J.S., and Dotti, C.G. (2002). Breaking the neuronal sphere: regulation of the actin cytoskeleton in neuritogenesis. Nat. Rev. Neurosci. *3*, 694–704.

Dehmelt, L., Smart, F.M., Ozer, R.S., and Halpain, S. (2003). The role of microtubule-associated protein 2c in the reorganization of microtubules and lamellipodia during neurite initiation. J. Neurosci. *23*, 9479–9490.

Delorme, V., Machacek, M., DerMardirossian, C., Anderson, K.L., Wittmann, T., Hanein, D., Waterman-Storer, C., Danuser, G., and Bokoch, G.M. (2007). Cofilin activity downstream of Pak1 regulates cell protrusion efficiency by organizing lamellipodium and lamella actin networks. Dev. Cell *13*, 646–662.

Dent, E.W., Kwiatkowski, A.V., Mebane, L.M., Philippar, U., Barzik, M., Rubinson, D.A., Gupton, S., Van Veen, J.E., Furman, C., Zhang, J., et al. (2007). Filopodia are required for cortical neurite initiation. Nat. Cell Biol. *9*, 1347–1359.

Dent, E.W., Gupton, S.L., and Gertler, F.B. (2011). The growth cone cytoskeleton in axon outgrowth and guidance. Cold Spring Harb. Perspect. Biol. *3*, 3.

Dotti, C.G., Sullivan, C.A., and Banker, G.A. (1988). The establishment of polarity by hippocampal neurons in culture. J. Neurosci. *8*, 1454–1468.

Edson, K., Weisshaar, B., and Matus, A. (1993). Actin depolymerisation induces process formation on MAP2-transfected non-neuronal cells. Development *117*, 689–700.

Endo, M., Ohashi, K., Sasaki, Y., Goshima, Y., Niwa, R., Uemura, T., and Mizuno, K. (2003). Control of growth cone motility and morphology by LIM

(B) Quantification of retrograde actin flow in wild-type, *AC KO* control, *AC KO* + CofY82F-RFP, and *AC KO* + CofS94D-RFP neurons; n ≥ 20 cells for each condition.
(C) Micrographs of RFP and βIII-tubulin staining of *AC KO* neurons expressing RFP, CofS94D-RFP, or CofY82F-RFP at 2 DIV. CofY82F-RFP expression results in a rescue of neurite formation (arrowheads). Scale bar represents 20 μm.
(D) Quantification of the developmental stages in wild-type + RFP-, *AC KO* + RFP-, *AC KO* + CofS94D-RFP-, and *AC KO* + CofY82F-RFP-expressing neurons. n ≥ 150 cells from three experiments at 2 DIV.
(E) Quantification of the percentage of cells with filopodia in stage 1 neurons. n ≥ 90 cells from three experiments.
*p < 0.05, **p < 0.01, ***p < 0.001. Error bars represent SD.
(F) In wild-type brain, ADF/Cofilin (AC) activity directs neuritogenesis. After terminal mitotic division, a newborn neuron in the ventricular zone/subventricular zone (VZ/SVZ) undergoes neurite formation. ADF/Cofilin (yellow) binds to the ADP-actin (dark red) portion of F-actin and promotes severing of the filaments (Pac-Man). This increases actin turnover and facilitates the radial arrangement of actin filaments (red), which frees space for radial microtubule (green) growth and coalescence, leading to the formation of a nascent neurite.
(G) In the *AC KO* brain, neuritogenesis is severely attenuated due to dense and disordered F-actin and abnormal microtubule growth. IZ, intermediate zone; CP, cortical plate.

kinase and Slingshot via phosphorylation and dephosphorylation of cofilin. J. Neurosci. *23*, 2527–2537.

Flynn, K.C., Pak, C.W., Shaw, A.E., Bradke, F., and Bamburg, J.R. (2009). Growth cone-like waves transport actin and promote axonogenesis and neurite branching. Dev. Neurobiol. *69*, 761–779.

Forscher, P., and Smith, S.J. (1988). Actions of cytochalasins on the organization of actin filaments and microtubules in a neuronal growth cone. J. Cell Biol. *107*, 1505–1516.

Garvalov, B.K., Flynn, K.C., Neukirchen, D., Meyn, L., Teusch, N., Wu, X., Brakebusch, C., Bamburg, J.R., and Bradke, F. (2007). Cdc42 regulates cofilin during the establishment of neuronal polarity. J. Neurosci. *27*, 13117–13129.

Goebbels, S., Bormuth, I., Bode, U., Hermanson, O., Schwab, M.H., and Nave, K.A. (2006). Genetic targeting of principal neurons in neocortex and hippocampus of NEX-Cre mice. Genesis *44*, 611–621.

Heng, J.I., Chariot, A., and Nguyen, L. (2010). Molecular layers underlying cytoskeletal remodelling during cortical development. Trends Neurosci. *33*, 38–47.

Hotulainen, P., Paunola, E., Vartiainen, M.K., and Lappalainen, P. (2005). Actin-depolymerizing factor and cofilin-1 play overlapping roles in promoting rapid F-actin depolymerization in mammalian nonmuscle cells. Mol. Biol. Cell *16*, 649–664.

Jiang, X.S., Wassif, C.A., Backlund, P.S., Song, L., Holtzclaw, L.A., Li, Z., Yergey, A.L., and Porter, F.D. (2010). Activation of Rho GTPases in Smith-Lemli-Opitz syndrome: pathophysiological and clinical implications. Hum. Mol. Genet. *19*, 1347–1357.

Korets-Smith, E., Lindemann, L., Tucker, K.L., Jiang, C., Kabacs, N., Belteki, G., Haigh, J., Gertsenstein, M., and Nagy, A. (2004). Cre recombinase specificity defined by the tau locus. Genesis *40*, 131–138.

Korobova, F., and Svitkina, T. (2008). Arp2/3 complex is important for filopodia formation, growth cone motility, and neuritogenesis in neuronal cells. Mol. Biol. Cell *19*, 1561–1574.

Kwiatkowski, A.V., Rubinson, D.A., Dent, E.W., Edward van Veen, J., Leslie, J.D., Zhang, J., Mebane, L.M., Philippar, U., Pinheiro, E.M., Burds, A.A., et al. (2007). Ena/VASP Is Required for neuritogenesis in the developing cortex. Neuron *56*, 441–455.

Loisel, T.P., Boujemaa, R., Pantaloni, D., and Carlier, M.F. (1999). Reconstitution of actin-based motility of Listeria and Shigella using pure proteins. Nature *401*, 613–616.

Lowery, L.A., and Van Vactor, D. (2009). The trip of the tip: understanding the growth cone machinery. Nat. Rev. Mol. Cell Biol. *10*, 332–343.

Lu, M., Witke, W., Kwiatkowski, D.J., and Kosik, K.S. (1997). Delayed retraction of filopodia in gelsolin null mice. J. Cell Biol. *138*, 1279–1287.

Luby-Phelps, K., and Taylor, D.L. (1988). Subcellular compartmentalization by local differentiation of cytoplasmic structure. Cell Motil. Cytoskeleton *10*, 28–37.

Medeiros, N.A., Burnette, D.T., and Forscher, P. (2006). Myosin II functions in actin-bundle turnover in neuronal growth cones. Nat. Cell Biol. *8*, 215–226.

Michelot, A., Berro, J., Guérin, C., Boujemaa-Paterski, R., Staiger, C.J., Martiel, J.L., and Blanchoin, L. (2007). Actin-filament stochastic dynamics mediated by ADF/cofilin. Curr. Biol. *17*, 825–833.

Moriyama, K., and Yahara, I. (1999). Two activities of cofilin, severing and accelerating directional depolymerization of actin filaments, are affected differentially by mutations around the actin-binding helix. EMBO J. *18*, 6752–6761.

Moriyama, K., and Yahara, I. (2002). The actin-severing activity of cofilin is exerted by the interplay of three distinct sites on cofilin and essential for cell viability. Biochem. J. *365*, 147–155.

Pak, C.W., Flynn, K.C., and Bamburg, J.R. (2008). Actin-binding proteins take the reins in growth cones. Nat. Rev. Neurosci. *9*, 136–147.

Petchprayoon, C., Suwanborirux, K., Tanaka, J., Yan, Y., Sakata, T., and Marriott, G. (2005). Fluorescent kabiramides: new probes to quantify actin in vitro and in vivo. Bioconjug. Chem. *16*, 1382–1389.

Rasband, M.N. (2010). The axon initial segment and the maintenance of neuronal polarity. Nat. Rev. Neurosci. *11*, 552–562.

Riedl, J., Flynn, K.C., Raducanu, A., Gärtner, F., Beck, G., Bösl, M., Bradke, F., Massberg, S., Aszodi, A., Sixt, M., and Wedlich-Söldner, R. (2010). Lifeact mice for studying F-actin dynamics. Nat. Methods *7*, 168–169.

Roland, J., Berro, J., Michelot, A., Blanchoin, L., and Martiel, J.L. (2008). Stochastic severing of actin filaments by actin depolymerizing factor/cofilin controls the emergence of a steady dynamical regime. Biophys. J. *94*, 2082–2094.

Saarikangas, J., Zhao, H., and Lappalainen, P. (2010). Regulation of the actin cytoskeleton-plasma membrane interplay by phosphoinositides. Physiol. Rev. *90*, 259–289.

Saito, T. (2006). In vivo electroporation in the embryonic mouse central nervous system. Nat. Protoc. *1*, 1552–1558.

Schaefer, A.W., Schoonderwoert, V.T., Ji, L., Mederios, N., Danuser, G., and Forscher, P. (2008). Coordination of actin filament and microtubule dynamics during neurite outgrowth. Dev. Cell *15*, 146–162.

Small, J.V., and Resch, G.P. (2005). The comings and goings of actin: coupling protrusion and retraction in cell motility. Curr. Opin. Cell Biol. *17*, 517–523.

Stiess, M., and Bradke, F. (2011). Neuronal polarization: The cytoskeleton leads the way. Dev. Neurobiol. *71*, 430–444.

Tahirovic, S., Hellal, F., Neukirchen, D., Hindges, R., Garvalov, B.K., Flynn, K.C., Stradal, T.E., Chrostek-Grashoff, A., Brakebusch, C., and Bradke, F. (2010). Rac1 regulates neuronal polarization through the WAVE complex. J. Neurosci. *30*, 6930–6943.

Witte, H., Neukirchen, D., and Bradke, F. (2008). Microtubule stabilization specifies initial neuronal polarization. J. Cell Biol. *180*, 619–632.